Received 11 February 2022; accepted 28 February 2022. Date of publication 3 March 2022; date of current version 15 March 2022.

*Digital Object Identifier 10.1109/OJCOMS.2022.3156382*

# Analog Radio Over Fiber-Aided Multi-Service Communications for High-Speed Trains

**YICHUAN LI [1], SALMAN GHAFOOR [2], AND MOHAMMED EL-HAJJAR [3] (Senior Member, IEEE)**

[1]Department of Electronics and Information, Harbin Institute of Technology (Shenzhen), Shenzhen 518055, China

[2]School of Electrical Engineering and Computer Science, National University of Sciences and Technology, Islamabad 44000, Pakistan

[3]School of Electronics and Computer Science, University of Southampton, Southampton SO17 1BJ, U.K.

CORRESPONDING AUTHOR: Y. LI (e-mail: liyichuan@hit.edu.cn)

This work was supported in part by the Shenzhen Scientific Research Foundation for the Introduction of High-Caliber Personnel under Grant JB11409017; in part by the Shenzhen Postdoctoral Science Foundation under Grant JB25501024; and in part by the Research Foundation of HITsz under Grant JB45001037.

**ABSTRACT** High speed trains (HST) have gradually become an essential means of transportation, where given our digital world, it is expected that passengers will be connected all the time. More specifically, the on-board passengers require fast mobile connections, which cannot be provided by the currently implemented cellular networks. Hence, in this article, we propose an analogue radio over fiber (A-RoF) aided multi-service network architecture for high-speed trains, in order to enhance the quality of service as well as reduce the cost of the radio access network (RAN). The proposed design can simultaneously support sub-6GHz as well as millimetre wave (mmWave) communications using the same architecture. Explicitly, we design a photonics aided beamforming technique in order to eliminate the bulky high-speed electronic phase-shifters and the hostile broadband mmWave mixers while providing a low-cost RAN solution. Finally, a beamforming range of 180° is demonstrated with a high resolution using our proposed system.

**INDEX TERMS** Optical fiber, radio access network, beyond 5G, high speed train, analogue radio over fiber, mmWave. beamforming.

## I. INTRODUCTION

THE HIGH speed train (HST) operating at a speed above 300 km/hour has fundamentally changed the individuals' life-style. It is reported that HST has the second-highest Internet streaming after household environments, such as homes and offices [1], [2], where the majority of this streaming is used for supporting the on-board activities, such as on-demand video, online-gaming, and voice or video calling. Furthermore, since the 4G and 5G use the sub-6GHz band and then the millimeter wave (mmWave) communications will coexist with these frequency bands [3], a railway network supporting multi-service is required, where the passengers are capable of being connected to 4G, 5G, Beyond 5G or even Wi-Fi networks all the time [3]–[5]. On the other hand, HST has some specific requirements, such as requiring high capacity due to the high number of passengers in addition to the high Doppler effects caused by the high speed [6], [7]. As a result, this requires a higher number of base stations (BSs) with a more efficient cellular handover technique, which has several challenges [6]–[9]. First, the denser deployment of BSs can provide seamless connection for the passengers by increasing the capacity per cell, which, however, would impose more inter-cell interference (ICI) [6], [7]. Additionally, the severe Doppler effects significantly affect the communications network performance as the train is moving extremely fast, impacting the handover process of the cellular networks [4], [5]. Besides, the channel estimation might be less accurate due to the rapid channel variations, which can influence the quality of service (QoS) and hence, the user experience [8], [9].

As a solution, mmWave beamforming has been proposed for mitigating the ICI, while enhancing the capacity, especially in ultra-dense cellular networks [10]. Furthermore, two-hop relay communications are advocated by [1], [4] to address the handover failure and the rapid channel variation in HSTs, where several relay antennas can be installed

This work is licensed under a Creative Commons Attribution 4.0 License. For more information, see https://creativecommons.org/licenses/by/4.0/

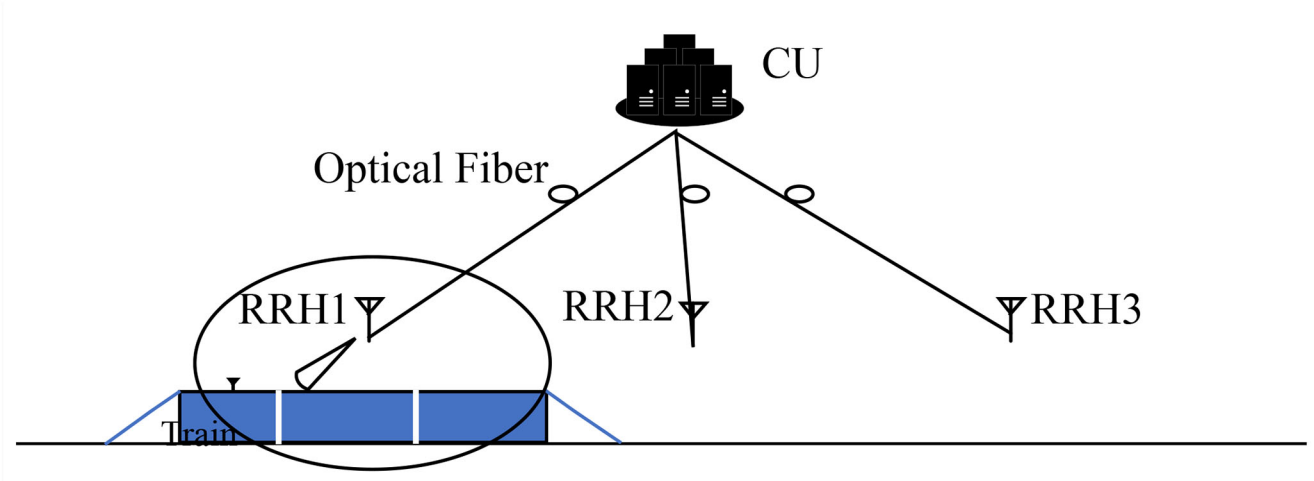


**FIGURE 1.** Multi-service HST System Architecture.

on the rooftop of the train cars for a stable handover by either wavelength division multiplexing (WDM) or optical switches. However, in order to have a decent quality of service (QoS), a large number of base-stations must be deployed, increasing the total cost of the radio access networks (RANs) including both the Capital Expenditure (CAPEX) and the Operational Expenditure (OPEX). Hence, ultra-light RANs are required [11]. In addition, mmWave communications beamforming requires high-speed mmWave phase-shifters [12], which increases the overall RAN cost and limits the tuning carrier frequency range [13]–[15], and the broadband mixers, which affects achievable the bit error rate (BER) performance [13]. Furthermore, the phase-shifter based beamforming would impose beam-squinting on the wideband signals.[1]

The analogue radio over (A-RoF) based true-time delay is a low-cost yet high-performance RAN solution with ultra-light remote radio head (RRH) [6], [14], [16]–[20], where the RAN is separated between the central unit (CU) and several RRHs and is capable of reducing both its power-consumption and complexity. Explicitly, the A-RoF aided beamformer was proposed for providing beam-squinting free beamforming using the uniform fiber Bragg grating (FBG) [15], [21], [22] or a single chirped FBG (CFBG) [23], [24]. Thus, we aim to deploy an access network for a high-speed train system, which requires ultra-light RRH deployment, where our system also meets the requirement of the Option 8 of the functional split defined by eCPRI, which is the 5G RAN standard [25], [26].

In this article, we design a two-hop HST communications network combined with the A-RoF aided beamforming techniques, where multi services are delivered to the train, such as on-demand video, online-gaming, and voice or video calling, which are carried by mmWave and sub-6GHz signals using 4G, 5G or Wi-Fi networks. Explicitly, the multi service signals generated in the CU of Fig. 1 are transmitted through a short-length fiber of upto 20km to the RRHs, which communicate with the antennas on the top of the HST to provide the required service to the on-board passengers. The beam pattern is controlled in the CU using the CFBG, instead of the costly and bulky phase-shifters in the RRHs, alleviating the size and cost of the RRH and facilitating the densely deployed RRHs along the railways. In contrast to the traditional digital radio over fiber, A-RoF has been proved to be more cost-effective, especially considering several aggregated radio signals such as multi-service signals [27]. The proposed system enables both cost-reduction by simplifying the RAN design and performance-improvement by exploiting centralised optical processing and multi-service signal generation as a benefit of the A-RoF architecture [14]. The novel contributions of our design are as follow:

1) *Photonic aided true-time delay beamforming:* We conceive a multi-service true-time-delay transmit beamforming for HST two-hop network, while also eliminating the beam-squinting phenomenon.
2) *Energy-efficient RRHs:* The large-scale power-thirsty phase shifters and costly mmWave phase shifters are removed, while the beam is optically controlled using the passive FBGs in the proposed design, hence improving the OPEX-savings and enabling ultra-light RRHs deployment. Furthermore, we compare the conventional system with our designed system, where we show that the number of total hardware for transmitting the multi-service signal and of the active optical components are reduced, resulting in the lower energy-consumption, leading to reduced total cost.
3) *Multi-service signal generation:* Multi-service signals carried by mmWave and sub-6GHz frequency band can be optically generated and beam-steered to the HST in the same direction.

1. Beamsquinting is the beam-shifts caused by the frequency shifts when applied with the constant phase-shift among neighbouring antenna element (AE). This would be even severe in the context of wide-band signal beamsteering [15].

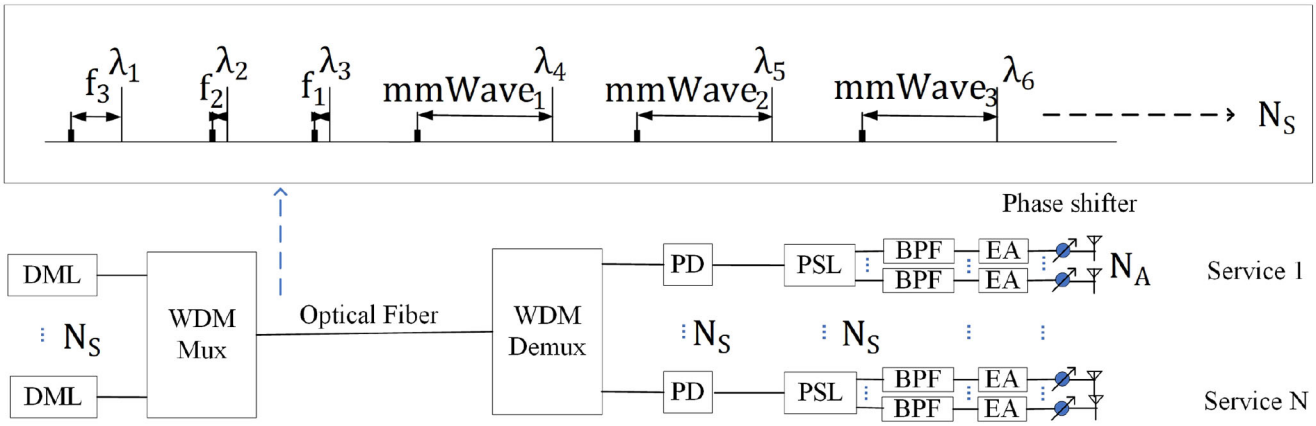


**FIGURE 2.** Conventional System Model (DML: Directly Modulated Laser; WDM Mux: Wavelength Division Multiplexer; PD, Photo-detector; PSL: Power Splitter; BPF: Bandpass Filter; EA: Electronic Amplifier; NS: Number of Services; NA: Number of Antenna Element).

4) *Centralised optical processing:* unlike the phase-shifter used in conventional wireless transmit beamforming, the beam control module is located in the central unit, potentially facilitating the coordinated multipoint (CoMP) transmission.

The rest of the paper is organised as follows. We introduce the multi-service two-hop train system in Section II, while the A-RoF aided beamforming technique and its time delay principle are detailed in Section III. Then, we present the cost-benefits and the beamforming performance of our proposed system in Section IV, followed by the conclusion in Section V.

## II. MULTI-SERVICE HST SYSTEM ARCHITECTURE

In this section, we present a general architecture for the two-hop HST system shown in Fig. 1, which can be exploited in our design. As shown in Fig. 1, the signal is generated in the CU and transmitted via fiber to several RRHs, where only optical-to-electronic conversion, amplification and filtering are performed, thus substantially reducing the RRH size. Explicitly, the RRH receives the signal from the CU using fiber and then transmits this signal to the HST using a set of antenna arrays, as shown in Fig. 1, where the RRHs are placed along the train line and will communicate with the antenna arrays on the rooftop of the HST.

The signals transmitted from the RRHs to the HST are beamformed and transmitted to the antenna arrays fixed on the rooftop of the HST, as shown in Fig. 1. Then, the signals are relayed to the on-board passengers to fulfil the users demands through the indoor communication system using multiple access techniques [28]. It has been verified using field tests that the two-hop relay communication in HST setup outperforms the conventional 4G cellular system in terms of signal quality [28].

Since the 4G and 5G signals would co-exist in the non-standalone 5G deployment proposed by the 3GPP in the recent Releases [29], multi-service signal transmission using different frequency bands and wireless standards are of importance to support the users' daily streaming, on-line gaming, voice or video call and on-demand video [3].

Conventionally, the A-RoF aided multi-service system can be supported using the architecture of Fig. 2 [1], [4], [9], [28], [30], where different services carried by different frequencies are directly modulated by individual lasers before being coupled into an optical fiber. At the end of the fiber, each optical and radio frequency (RF) chain are used for optical-to-electronic conversion, amplification, filterings. Furthermore, when analogue beamforming is employed for improving the signal-to-noise ratio performance, a large number of phase-shifters, band-pass filter (BPFs), electronic amplifiers (EAs) are required, which increases the cost and power-consumption of the whole system. Explicitly, let us take service 1 as an example, as shown in Fig. 2, assuming the RF of $f_3$ carries service 1, $f_3$ is used to directly modulate a laser operating at the center wavelength of $\lambda_1$. Then, coupled with other services carried by $\lambda_2$ to $\lambda_6$ into the fiber, the WDM signal of the spectrum shown in Fig. 2 feeds the optical fiber for transmission, after which the WDM Demultiplexer (WDM Demux) separates each wavelength. Then, the modulated optical signal of $\lambda_1$ is photo-detected and the $f_3$ carrying service 1 is recovered, followed by the power splitter (PSL) which splits the power of the RF frequency, where, each BPF and EA is used for filtering out the wanted signal and for the amplification of each port of the PSL, respectively. Finally, several phase-shifters are used to phase-shift each output to form a desired beam pattern, leading to the analogue beamforming with large amount of power-thirsty and bulky phase-shifter deployment. In the next section, we will introduce our A-RoF system based on the two-hop transmission, while invoking a lower-cost photonic aided multi-service solution. Note that our design focuses on the design of the interface between the CU and the RRH and not on the design of the wireless link to the HST on-board passengers, where the CU-RRH function that provides a low-cost and flexible multi-service RAN solution is presented in details in the next section.

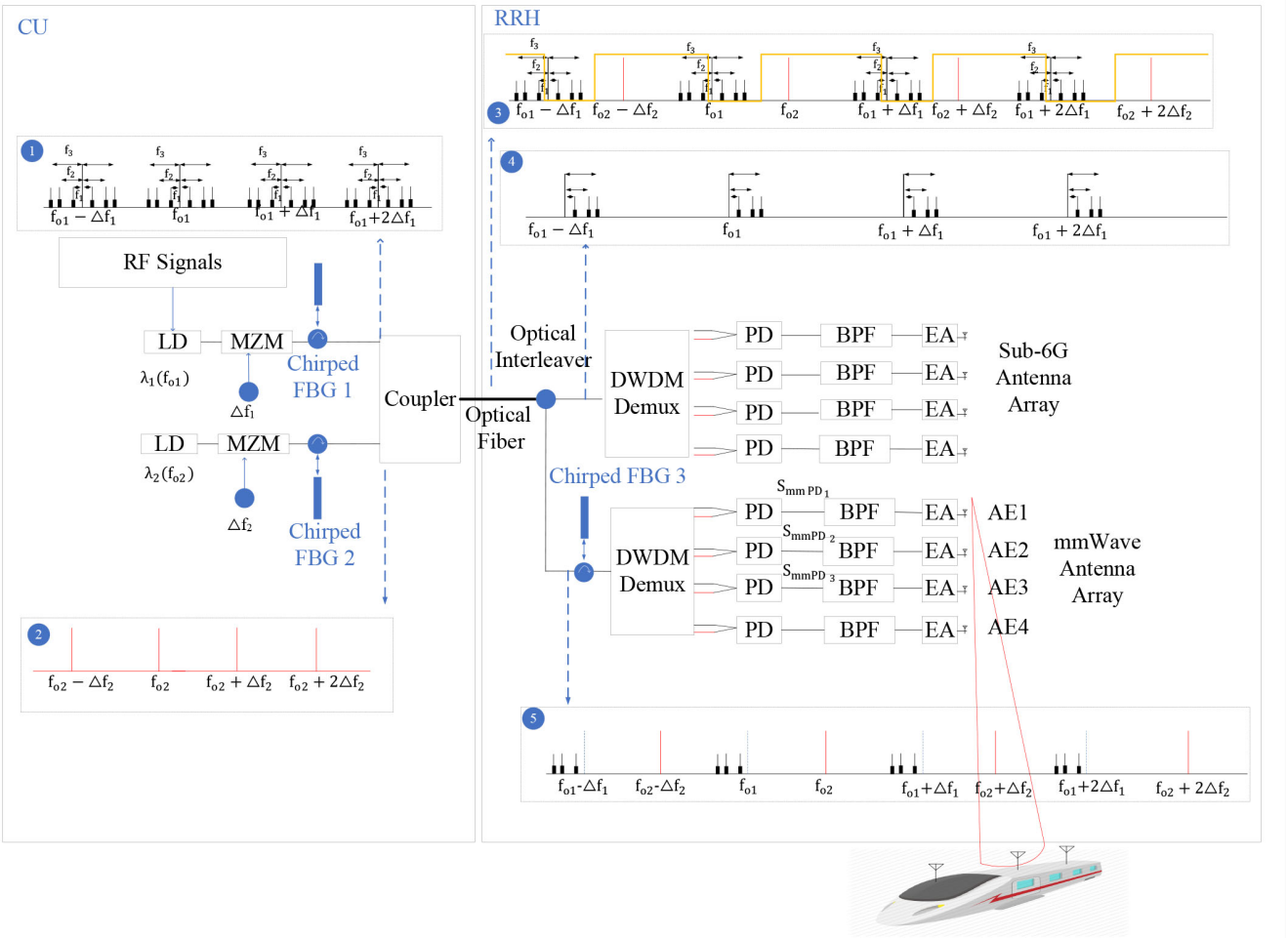


**FIGURE 3.** Proposed A-RoF aided Multi-service Architecture.

## III. A-ROF AIDED BEAMFORMING FOR HIGH-SPEED TRAIN MULTI-SERVICE COMMUNICATIONS

### A. A-ROF AIDED HST SYSTEM MODEL

As mentioned in Section II, the RRH beamforms the multi-service signals, composed of sub-6GHz and mmW signals, to the HST rooftop antenna arrays. Fig. 3 shows the proposed A-RoF design, where the sub-6GHz and mmW signals are beamformed in the same direction to the antenna array placed on the rooftop of the train. The proposed design avoids the beam-squinting as well as considers low-complexity RRH.

In Fig. 3, the access network is divided into CU and RRH, where the CU performs the baseband signal processing as well as the radio modulations [14], while the RRH is simplified to only radio functions such as amplifications and filtering. Explicitly, in the CU of Fig. 3, the RF signals of $f_1$, $f_2$ and $f_3$ directly modulate a laser diode (LD) operating at $\lambda_1$. The signal at the output of the directly modulated laser is given at the optical input of a Mach-Zehnder modulator (MZM) that is being driven by a sinusoidal signal of frequency $\Delta f_1$. The nonlinear transfer function of the MZM results in the generation of multiple spectral copies of the directly modulated optical signal having a frequency spacing of $\Delta f_1$ as shown in Fig. 3 [13]. The resulting WDM signal is time-delayed using a CFBG, which is capable of reflecting different wavelengths with a linear time-delay. Then, as shown in Fig. 3, another laser diode operating at $\lambda_2$ is intensity modulated by a sinusoidal signal having a frequency of $\Delta f_2$ by a MZM to generate multiple sidebands by using the nonlinear function of the MZM [13]. The two WDM signals are coupled into a single mode fiber using a fiber coupler as shown in Fig. 3.

As shown in the RRH of Fig. 3, the combined WDM signal is separated by a two-port optical interleaver, which filters the desired signals to two individual dense wavelength division demultiplexers (DWDM Demux), each of which would be used for either sub-6GHz signal generation or mmWave signal generation. The upper DWDM Demux of Fig. 3 filters the spectrum which can generate a beat frequency of sub-6GHz bands. Then, the photodetected sub-6GHz frequency after each PD is band-pass filtered and amplified, while the inter-element time delay is dependent on the chirped FBG 1 and FBG 2 strains as tested by [31]. Similarly, the bottom DWDM Demux in the RRH of Fig. 3 is used for mmWave signal generation, where an extra chirped FBG,

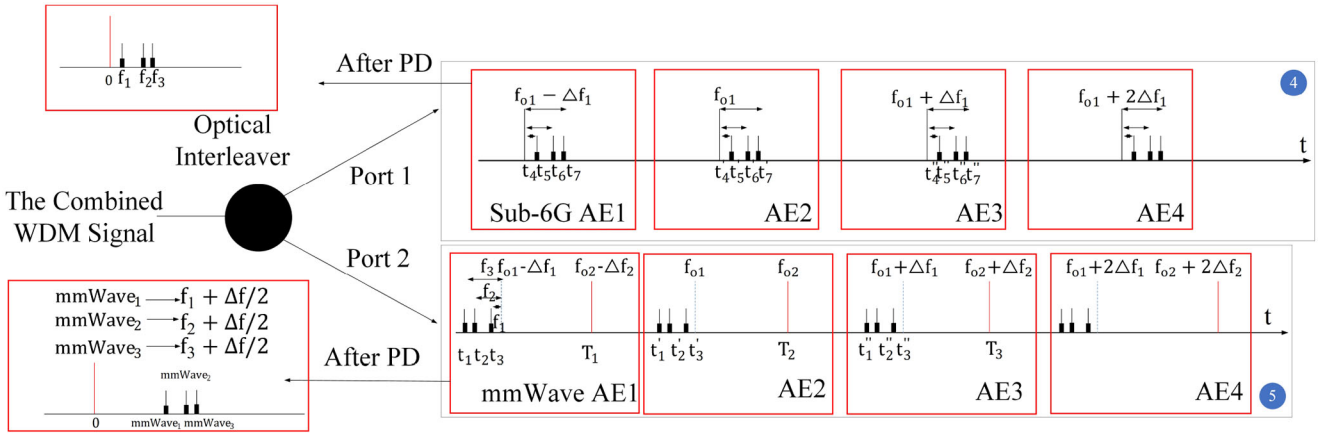


**FIGURE 4.** The proposed network's multi-service signal generation and their time-delay imposed.

namely chirped FBG 3 of Fig. 3, is implemented for adjusting the beam direction to be the same as the sub-6GHz bands, which will be elaborated in the next section.

To elaborate further on the RF and mmWave signals generation, as shown in Fig. 4, the optical interleaver, which is a periodic optical filter, separates the combined WDM signals of spectrum ③ of Fig. 3. The spectrum of the two outputs of the optical interleaver is depicted in Fig. 4, where port 1 maps the spectrum ④ of Fig. 4 to the sub-6GHz spectrum of $f_1$, $f_2$ and $f_3$, with port 2 mapping the spectrum ⑤ to the mmWave frequencies of $f_1 + \frac{\Delta f}{2}$, $f_2 + \frac{\Delta f}{2}$ and $f_3 + \frac{\Delta f}{2}$.[2] Let us now consider a four-antenna-element system for both the sub-6GHz and mmWave transmission. The beating frequencies of the red boxes of Fig. 4 would be mapped to antenna elements 1-4 of both the mmWave antenna array and the sub-6GHz antenna array dispensing with the mmWave mixers and phase shifters, since they have been performed using the above optical link with the aid of WDM signal and CFBG.

Thus, a multi-service communication system transporting sub-6GHz and mmWave signals in the same direction is built for the two-hop HST systems. In the next section, we will detail the true-time delay principles and its mapping rule from the optical domain to the electronic domain as well as the multi-service generation.

### B. TRUE-TIME DELAY PRINCIPLE

Instead of exploiting the conventional phase-shifting schemes for analogue beamforming [32], our proposed system invokes the true-time delay, which relies on the constant time-delay among the RF signal fed into the adjacent antennas elements to introduce the beam steering, which is capable of mitigating the wide-band beam-squinting problems [15]. While undermining the codebook design of the phased-array systems [33], beam-squinting is also detrimental for the channel estimation and precoding, which further degrades the wireless communication transmission rate [34].

In the following, with the aid of the mathematical derivation, we will prove how the imposed optical linear time-delay is used for introducing the constant time-delay among the RF signal fed into the adjacent antennas elements of each antenna array of Fig. 3. In the upper line of the CU in Fig. 3, where the spectrum ① is generated, the multi-service RF signals are used to directly modulate a laser diode and the input optical field of the MZM can be formulated as [13]:

$$E_{in}(t) = \sqrt{P_{Laser}} e^{j\omega_{\lambda_1} t}\big[1 + cos(\omega_{f_1} t) + cos(\omega_{f_2} t) + cos(\omega_{f_3} t)\big], \quad (1)$$

where $P_{Laser}$ is the LD output power and $\omega_{f_1}$, $\omega_{f_2}$ and $\omega_{f_3}$ denote the optical carrier's angular frequency corresponding to $\lambda_1$, $\lambda_2$ and $\lambda_3$ of Fig. 3. Then, the MZM output field [13] is as follows:

$$\begin{aligned}
E_{MZM_{up}}(t) &= cos\left(\pm\frac{\pi}{4} + \frac{\pi V_{dr} cos(\omega_{\Delta f_1})}{2V_\pi}\right) E_{in}(t) \\
&= \frac{\sqrt{P_{laser}}[1 + cos(\omega_{f_1} t) + cos(\omega_{f_2} t) + cos(\omega_{f_3} t)]e^{j\omega_{\lambda_1} t}}{\sqrt{2}} \\
&\quad \left[J_0\left(\frac{\pi |V_{dr}|}{2V_\pi}\right) + 2\sum_{n=1}^{\infty}(-1)^n J_{2n}\left(\frac{\pi V_{dr}}{2V_\pi}\right) cos(2n\omega_{\Delta f_1} t)\right. \\
&\quad \left. \pm 2\sum_{n=1}^{\infty}(-1)^n J_{2n-1}\left(\frac{\pi V_{dr}}{2V_\pi}\right) cos((2n-1)\omega_{\Delta f_1} t)\right] \\
&= \frac{\sqrt{P_{laser}}}{\sqrt{2}}\left[J_0\left(\frac{\pi |V_{dr}|}{2V_\pi}\right)\left[e^{j\omega_{\lambda_1} t} + e^{j(\omega_{\lambda_1}+\omega_{f_1})t}/2\right.\right. \\
&\quad + e^{j(\omega_{\lambda_1} t - \omega_{f_1} t)}/2 + e^{j(\omega_{\lambda_1}+\omega_{f_2})t}/2 + e^{j(\omega_{\lambda_1} t - \omega_{f_2} t)}/2 \\
&\quad \left.\left. + e^{j(\omega_{\lambda_1}+\omega_{f_3})t}/2 + e^{j(\omega_{\lambda_1} t - \omega_{f_3} t)}/2\right]\right. \\
&\quad + 2\sum_{n=1}^{\infty}(-1)^n J_{2n}\left(\frac{\pi V_{dr}}{2V_\pi}\right) \\
&\quad \times\left[e^{j(\omega_{\lambda_1}+2n\omega_{\Delta f_1})t}/2 + e^{j(\omega_{\lambda_1}-2n\omega_{\Delta f_1})t}/2\right.
\end{aligned}$$

2. Note that if $\frac{\Delta f}{2} = f_{o1} - f_{o2}$ is upto 25 GHz, $f_1 + \frac{\Delta f}{2}$ is the mmWave signal of at least 25 GHz. The spectrum ④ and ⑤ of Fig. 4 corresponds to spectrum ④ and ⑤ of Fig. 3.

$$
\begin{aligned}
&+\frac{e^{j(\omega_{\lambda_1}+2n\omega_{\Delta f_1}+\omega_{f_1})t}/2+e^{j(\omega_{\lambda_1}-2n\omega_{\Delta f_1}-\omega_{f_1})t}/2}{2}\\
&+\frac{e^{j(\omega_{\lambda_1}+2n\omega_{\Delta f_1}-\omega_{f_1})t}/2+e^{j(\omega_{\lambda_1}-2n\omega_{\Delta f_1}+\omega_{f_1})t}/2}{2}\\
&+\frac{e^{j(\omega_{\lambda_1}+2n\omega_{\Delta f_1}+\omega_{f_2})t}/2+e^{j(\omega_{\lambda_1}-2n\omega_{\Delta f_1}-\omega_{f_2})t}/2}{2}\\
&+\frac{e^{j(\omega_{\lambda_1}+2n\omega_{\Delta f_1}-\omega_{f_2})t}/2+e^{j(\omega_{\lambda_1}-2n\omega_{\Delta f_1}+\omega_{f_2})t}/2}{2}\\
&+\frac{e^{j(\omega_{\lambda_1}+2n\omega_{\Delta f_1}+\omega_{f_3})t}/2+e^{j(\omega_{\lambda_1}-2n\omega_{\Delta f_1}-\omega_{f_3})t}/2}{2}\\
&+\frac{e^{j(\omega_{\lambda_1}+2n\omega_{\Delta f_1}-\omega_{f_3})t}/2+e^{j(\omega_{\lambda_1}-2n\omega_{\Delta f_1}+\omega_{f_3})t}/2}{2}\Bigg]\\
&\pm 2\sum_{n=1}^{\infty}(-1)^n J_{2n-1}\left(\frac{\pi V_{dr}}{2V_\pi}\right)\\
&\times\Bigg[\frac{e^{j(\omega_{\lambda_1}+(2n-1)\omega_{\Delta f_1})t}+e^{j(\omega_{\lambda_1}-(2n-1)\omega_{\Delta f_1})t}}{2}\\
&\quad+\frac{e^{j(\omega_{\lambda_1}+(2n-1)\omega_{\Delta f_1}+\omega_{f_1})t}/2+e^{j(\omega_{\lambda_1}-(2n-1)\omega_{\Delta f_1}-\omega_{f_1})t}/2}{2}\\
&\quad+\frac{e^{j(\omega_{\lambda_1}+(2n-1)\omega_{\Delta f_1}-\omega_{f_1})t}/2+e^{j(\omega_{\lambda_1}-(2n-1)\omega_{\Delta f_1}+\omega_{f_1})t}/2}{2}\\
&\quad+\frac{e^{j(\omega_{\lambda_1}+(2n-1)\omega_{\Delta f_1}+\omega_{f_2})t}/2+e^{j(\omega_{\lambda_1}-(2n-1)\omega_{\Delta f_1}-\omega_{f_2})t}/2}{2}\\
&\quad+\frac{e^{j(\omega_{\lambda_1}+(2n-1)\omega_{\Delta f_1}-\omega_{f_2})t}/2+e^{j(\omega_{\lambda_1}-(2n-1)\omega_{\Delta f_1}+\omega_{f_2})t}/2}{2}\\
&\quad+\frac{e^{j(\omega_{\lambda_1}+(2n-1)\omega_{\Delta f_1}+\omega_{f_3})t}/2+e^{j(\omega_{\lambda_1}-(2n-1)\omega_{\Delta f_1}-\omega_{f_3})t}/2}{2}\\
&\quad+\frac{e^{j(\omega_{\lambda_1}+(2n-1)\omega_{\Delta f_1}-\omega_{f_3})t}/2+e^{j(\omega_{\lambda_1}-(2n-1)\omega_{\Delta f_1}+\omega_{f_3})t}/2}{2}\Bigg]\Bigg],
\end{aligned}
$$

where $\omega_{\Delta f_1}$, $V_{dr}$ and $V_{pi}$ are the angular frequency of $\Delta f_1$, the amplitude of the drive frequency of the MZM and its switching voltage. $J_n(\frac{\pi V_{dr}}{2V_\pi})$ is the Bessel function of the first kind and order n, which determines both the number and the amplitude of the side-bands. The spectrum of the MZM output is marked as ① of Fig. 3, where the same RF signals subsuming $f_1$, $f_2$ and $f_3$ are carried by each wavelength, generating a WDM signal spaced with $\Delta f_1$. Similarly, the WDM signal at the output of the second MZM represented by spectrum ② in Fig. 3 can be expressed as follows, where the input optical field of the bottom MZM $E_{in2}(t)$ and an unmodulated WDM signal $E_{MZM_{bottom}}(t)$ is generated:

$$
\begin{aligned}
&E_{in2}(t)=\sqrt{P_{Laser}}e^{j\omega_{\lambda_2}t}, \qquad (2)\\
&E_{MZM_{bottom}}(t)=cos\left(\pm\frac{\pi}{4}+\frac{\pi V_{dr}cos(\omega_{\Delta f_2})}{2V_\pi}\right)E_{in2}(t)\\
&=\frac{\sqrt{P_{laser}}e^{j\omega_{\lambda_2}t}}{\sqrt{2}}\Bigg[J_0\left(\frac{\pi V_{dr}}{2V_\pi}\right)2\sum_{n=1}^{\infty}(-1)^n J_{2n}+\left(\frac{\pi V_{dr}}{2V_\pi}\right)\\
&\qquad\times cos(2n\omega_{\Delta f_2}t)\pm 2\sum_{n=1}^{\infty}(-1)^n J_{2n-1}\\
&\qquad\times\left(\frac{\pi V_{dr}}{2V_\pi}\right)cos((2n-1)\omega_{\Delta f_2}t)\Bigg]\\
&=\frac{\sqrt{P_{laser}}}{\sqrt{2}}\Bigg[J_0\left(\frac{\pi|V_{dr}|}{2V_\pi}\right)\left(e^{j\omega_{\lambda_2}t}\right)\\
&\qquad+2\sum_{n=1}^{\infty}(-1)^n J_{2n}\left(\frac{\pi V_{dr}}{2V_\pi}\right)\\
&\qquad\times\left[e^{j(\omega_{\lambda_2}+2n\omega_{\Delta f_2})t}/2+e^{j(\omega_{\lambda_2}-2n\omega_{\Delta f_2})t}/2\right]\\
&\qquad\pm 2\sum_{n=1}^{\infty}(-1)^n J_{2n-1}\left(\frac{\pi V_{dr}}{2V_\pi}\right)\\
&\qquad\times\left[\frac{e^{j(\omega_{\lambda_2}+(2n-1)\omega_{\Delta f_2})t}+e^{j(\omega_{\lambda_2}-(2n-1)\omega_{\Delta f_2})t}}{2}\right]\Bigg].
\end{aligned}
$$

(3)

Then, the two WDM signals are combined using the fiber coupler and transmitted through a single mode fiber. By assuming $\Delta f=\Delta f_1=\Delta f_2$ and $\Delta f=2(f_{02}-f_{01})$, the combined WDM signal has a wavelength spacing of $\frac{\Delta f}{2}$. As shown in spectrum ③ of Fig. 3, the combined WDM signal would be filtered to two ports, with each being fed into a WDM Demux. Each output of the DWDM Demux would be fed into a photo detector to obtain either sub-6GHz signal or mmWave signal. Then, assuming the time delays imposed in the different frequencies are $t_n$ and $T_n$ as shown in Fig. 4 and by filtering the unwanted low frequency, we are capable of obtaining three frequencies in the mmWave spectrum as $S_{mmPD_1}$, $S_{mmPD_2}$ and $S_{mmPD_3}$ after the PD as shown in Fig. 3, which are then input to a BPF and then EA.[3] These mmWave signals can be represented as follows:

$$
\begin{aligned}
S_{mmPD_1}=\frac{P_{laser}}{2}\Bigg(&cos\Bigg(\left(\omega_{\lambda_2}-\omega_{\lambda_1}+\omega_{f_1}\right)\\
&\times\left(t+\frac{\omega_{\lambda_2}T_1-\omega_{\Delta f}T_1-\omega_{\lambda_1}t_3+\omega_{\Delta f}t_3+\omega_{f_1}t_3}{-\left(\omega_{\lambda_2}-\omega_{\lambda_1}+\omega_{f_1}\right)}\right)\Bigg)\\
&+cos\Bigg(\left(\omega_{\lambda_2}-\omega_{\lambda_1}+\omega_{f_2}\right)\\
&\times\left(t+\frac{\omega_{\lambda_2}T_1-\omega_{\Delta f}T_1-\omega_{\lambda_1}t_2+\omega_{\Delta f}t_2+\omega_{f_2}t_2}{-\left(\omega_{\lambda_2}-\omega_{\lambda_1}+\omega_{f_2}\right)}\right)\Bigg)\\
&+cos\Bigg(\left(\omega_{\lambda_2}-\omega_{\lambda_1}+\omega_{f_3}\right)\\
&\times\left(t+\frac{\omega_{\lambda_2}T_1-\omega_{\Delta f}T_1-\omega_{\lambda_1}t_1+\omega_{\Delta f}t_1+\omega_{f_3}t_1}{-\left(\omega_{\lambda_2}-\omega_{\lambda_1}+\omega_{f_3}\right)}\right)\Bigg)\Bigg)
\end{aligned}
$$

(4)

$$
\begin{aligned}
S_{mmPD_2}=\frac{P_{laser}}{2}\Bigg(&cos\Bigg(\left(\omega_{\lambda_2}-\omega_{\lambda_1}+\omega_{f_1}\right)\\
&\times\left(t+\frac{\omega_{\lambda_2}T_2-\omega_{\lambda_1}t_3^{'}+\omega_{f_1}t_3^{'}}{-\left(\omega_{\lambda_2}-\omega_{\lambda_1}+\omega_{f_1}\right)}\right)\Bigg)\\
&+cos\left(\left(\omega_{\lambda_2}-\omega_{\lambda_1}+\omega_{f_2}\right)\left(t+\frac{\omega_{\lambda_2}T_2-\omega_{\lambda_1}t_2^{'}+\omega_{f_2}t_2^{'}}{-\left(\omega_{\lambda_2}-\omega_{\lambda_1}+\omega_{f_2}\right)}\right)\right)
\end{aligned}
$$

3. Here, we use three photo-detected signals as an example, which can be readily extended to any number of photo detectors.

$$+ cos\left(\left(\omega_{\lambda_2} - \omega_{\lambda_1} + \omega_{f_3}\right)\left(t + \frac{\omega_{\lambda_2} T_2 - \omega_{\lambda_1} t_1^{'} + \omega_{f_3} t_1^{'}}{-\left(\omega_{\lambda_2} - \omega_{\lambda_1} + \omega_{f_3}\right)}\right)\right)\Bigg) \tag{5}$$

$$\begin{aligned} S_{mmPD_3} = \frac{P_{laser}}{2}\Bigg( & cos\Bigg(\left(\omega_{\lambda_2} - \omega_{\lambda_1} + \omega_{f_1}\right) \\ & \times \left(t + \frac{\omega_{\lambda_2} T_3 + \omega_{\Delta f} T_3 - \omega_{\lambda_1} t_3^{''} - \omega_{\Delta f} t_3^{''} + \omega_{f_1} t_3^{''}}{-\left(\omega_{\lambda_2} - \omega_{\lambda_1} + \omega_{f_1}\right)}\right)\Bigg) \\ & + cos\Bigg(\left(\omega_{\lambda_2} - \omega_{\lambda_1} + \omega_{f_2}\right) \\ & \quad \times \left(t + \frac{\omega_{\lambda_2} T_3 + \omega_{\Delta f} T_3 - \omega_{\lambda_1} t_2^{''} - \omega_{\Delta f} t_2^{''} + \omega_{f_2} t_2^{''}}{-\left(\omega_{\lambda_2} - \omega_{\lambda_1} + \omega_{f_2}\right)}\right)\Bigg) \\ & + cos\Bigg(\left(\omega_{\lambda_2} - \omega_{\lambda_1} + \omega_{f_3}\right) \\ & \quad \times \left(t + \frac{\omega_{\lambda_2} T_3 + \omega_{\Delta f} T_3 - \omega_{\lambda_1} t_1^{''} - \omega_{\Delta f} t_1^{''} + \omega_{f_3} t_1^{''}}{-\left(\omega_{\lambda_2} - \omega_{\lambda_1} + \omega_{f_3}\right)}\right)\Bigg)\Bigg), \end{aligned} \tag{6}$$

where $\omega_{mmWave_n} = \omega_{\lambda_2} - \omega_{\lambda_1} + \omega_{f_n}$ is the generated mmWave signal frequency. Then, if we take $\omega_{mmWave_1}$ as an example, according to Equations (4), (5) and (6), the time-delay difference between AE2 and AE1 can be referred to as $\Delta_1$, and between AE3 and AE2 as $\Delta_2$, which can be represented as:

$$\begin{aligned} \Delta_1 &= \frac{\omega_{\lambda_2} T_2 - \omega_{\lambda_1} t_3^{'} + \omega_{f_1} t_3^{'}}{-\left(\omega_{\lambda_2} - \omega_{\lambda_1} + \omega_{f_1}\right)} \\ &\quad - \frac{\omega_{\lambda_2} T_1 - \omega_{\Delta f} T_1 - \omega_{\lambda_1} t_3 + \omega_{\Delta f} t_3 + \omega_{f_1} t_3}{-\left(\omega_{\lambda_2} - \omega_{\lambda_1} + \omega_{f_1}\right)} \\ &= \frac{\omega_{mmWave_1}(T_2 - T_1) + (n(T_2 - T_1)/(2\pi))\left(2\pi\omega_{mmWave_1}/n\right)}{-\omega_{mmWave_1}} \\ &= -2(T_2 - T_1), \end{aligned} \tag{7}$$

and

$$\begin{aligned} \Delta_2 &= \frac{\omega_{\lambda_2}(T_3 - T_2) - \omega_{\lambda_1}\left(t_3^{''} - t_3^{'}\right) + \omega_{f_1}\left(t_3{}'' - t_3^{'}\right) + \omega_{\Delta f}\left(T_3 - t_3^{''}\right)}{-\left(\omega_{\lambda_2} - \omega_{\lambda_1} + \omega_{f_1}\right)} \\ &= -2(T_3 - T_2). \end{aligned} \tag{8}$$

As mentioned in Section I, CFBG is capable of obtaining a linear relation between the time delay and the optical spectrum fed into it, which would be elaborated in Section IV. Then, we obtain $\Delta T = T_3 - T_2 = T_2 - T_1$ as the time-delay difference of two frequencies with a spacing of $\Delta f$. Hence, we conclude that the optical time-delay of $\Delta T$ can result in a $-2\Delta T$ constant time-delay difference among the neighbouring AEs as verified by (7) and (8). This rule also applies to $\omega_{mmWave_1}$ and $\omega_{mmWave_2}$. Similarly, by repeating the process of the above derivation, we can have the time-delay difference relationship in terms of sub-6GHz as $\tau = -2\Delta T$. Then, we attempt to solve the problem of the beam-squinting for the mmWave and the sub-6GHz signals, where we implement the CFBG3 of Fig. 3, where the beam angle and the time delay relation is as follows:

$$\tau = \frac{dcos(\theta)}{c}, \tag{9}$$

where the $\theta$ is the beam angle to the perpendicular orientation of the antenna array. In order to obtain the same beam direction for both mmWave and sub-6GHz, the time delay difference of the sub-6GHz and the mmWave service must satisfy the following: $cos(\theta_1) = cos(\theta_2) = c\tau_1/d_1 = c\tau_2/d_2$, where we have $\tau_2 = \frac{d_2\tau_1}{d_1}$, with $d_1$ and $d_2$ being the inter-element distance of each antenna array. The CFBG3 of the RRH is capable of tuning the time delay of the mmWave service from $\tau_1$ to $\tau_2$.

Therefore, by assuming a linear relation of $t = nf + m$ between the optical frequency and the time delay imposed by the CFBG1 and CFBG2 of the CU of Fig 3, where $n$ and $m$ are constants and the new linear relation imposed by the CFBG3 in the RRH is $t = fk + j$, we have a new relation of frequency and time-delay as $t = f(k+n) + m + j$ for the mmWave WDM signal. As mentioned above, we have the following relationship:

$$\tau_1 = -2(T_2 - T_1) = -2n\Delta f, \tag{10}$$

$$\tau_2 = -2(T_2^{new} - T_1^{new}) = -2(n+k)\Delta f. \tag{11}$$

Thus, $\frac{d_2\tau_1}{d_1} = -2(n+k)\Delta f$, and we obtain the relation $k = -\frac{d_2\tau_1}{2d_1\Delta f} - n = \frac{d_2 - d_1}{d_1}n$. Then, by simply tuning the CFBG3 of the RRH according to the CFBG1 and CFBG2 of the CU of Fig. 3 to the new relation as $t = fk + j$, the multi-service communications including sub-6GHz and mmWave can be beamsteered to the same direction. Note that the linear relation can be tuned by changing the supported beam's deflection as demonstrated in [31], resulting in a tunable chirp rate of the linear CFBG, which is capable of obtaining a linear true-time delay of the WDM signals [31].

*In this section, we verified mathematically that a double time-delay of the neighbouring wavelength of the WDM signal can be translated into the inter-element time-delay difference of the antenna array, justifying the feasibility of A-RoF aided beamforming control using optical true-time delays, while removing the electronic phase-shifters and avoiding the beam squints.* In the next section, we will evaluate our system in terms of cost and performance.

## IV. SYSTEM EVALUATION

In this section, the system evaluation of our proposed system of Fig. 3 is presented. We will compare the cost and complexity of the proposed system with that of the conventional system of Fig. 2, following by a beamforming

**TABLE 1.** RRH complexity comparison.

| Components | Proposed System | Conventional System |
|---|---|---|
| Passive Components | | |
| Optical Interleaver | 1 | 0 |
| CFBG | 1 | 0 |
| DWDM Demux | 2 | 1 |
| Active Components | | |
| PD | 8 ($2N_A$) | 6 ($N_s$) |
| BPF | 8 ($2N_A$) | 24 ($N_sN_A$) |
| EA | 8 ($2N_A$) | 24 ($N_sN_A$) |
| Phase shifters | 0 | 12 mmWave PSs+12 Sub-6GHz PS ($N_sN_A$) |
| PSL | 0 | 6 ($N_s$) |

**TABLE 2.** RRH complexity comparison.

| Simulation Parameters | Values |
|---|---|
| Number of Antenna Element ($N_A$) | 4 |
| Combined WDM Wavelength Spacing | 25 GHz |
| Length of the Chirped FBG | 40 mm |
| $f_1$, $f_2$ and $f_3$ | 3, 5, 6 GHz |
| $f_{o1}$, $f_{o2}$ | 193.500, 193.525 GHz |
| WDM Central Frequencies | 193.450, 193.475, 193.500, 193.525 GHz<br>193.550, 193.575, 193.600, 193.625 GHz |
| RF signal Generation ($N_s$) | 3, 5, 6, 28, 30, 31 GHz |
| Simulation Platform | Optisystem, OptiGrating |

analysis[4] of Fig. 3.

### A. COST AND COMPLEXITY ANALYSIS

In this section, we analyse the cost benefits of our proposed design over the conventional system, where the multi-service bands are modulated using 6 LDs and beam-steered using 6 sets of phase-shifter array as shown in Fig. 2. As mentioned above, our design benefits from its ultralight RRH design, hence reducing the power-consumption and the OPEX. As shown in Table 1, we list the number of components implemented in our proposed A-RoF system of Fig. 3 and the conventional system as shown in Fig. 2, where $N_S$ denotes the number of services while $N_A$ is the number of antenna elements of each antenna array. Assuming we transmit sub-6GHz spectrum of $f_1$, $f_2$ and $f_3$ and the mmWave frequencies of $f_1 + \frac{\Delta f}{2}$, $f_2 + \frac{\Delta f}{2}$ and $f_3 + \frac{\Delta f}{2}$ using the four-antenna-element array, it is shown in Table 1 that in the proposed design of Fig 3, in contrast to the conventional design of Fig. 2, the bulky phase-shifters and the power splitter are totally removed, while the number of BPF, EA is substantially reduced. Instead, some passive components such as optical interleaver, CFBG and an extra DWDM Demux are introduced, but the number of which is not dependent on either the services or the antenna elements. Explicitly, as seen in Table 1, regarding the active components, the power-thirsty phase-shifter and power splitters are reduced from 24 and 6 to 0 and 0, respectively, while the number of BPFs and EAs are decreased from 24 and 24 to 8 and 8, respectively, resulting in a reduced power-consumption in the RRH of Fig. 3. Therefore, we can conclude that the power-consumption can be substantially reduced with the removal of the phase-shifters and the introduction of the passive optical components, while the total hardware cost would be reduced due to the optical mmWave generation without using the mmWave phase-shifters, simplifying the BPF and the EA.

### B. BEAMFORMING PERFORMANCE ANALYSIS

As mentioned in Section III-B, beam squinting and its effect on the performance of communications systems has been presented in the literature [15]. In the following, we elaborate on our proposed design for multi-service and multi-user true time delay beamforming.

In this section, we present our performance results for the proposed system, where we employ a uniform linear antenna array having four elements. The simulation parameters are listed in Table II, where we model the fiber-link channel using the commercial simulation tools, namely Optisystem and Optigrating, which are prevalently exploited by the

4. The QoS degradation of A-RoF compared to the digital solution is not presented in this paper since we focused on the beamforming design using the proposed A-RoF system. However, this issue has been widely investigated and demonstrated in our recent papers [16], [19], [35] as well as other literatures [36], [37], where it is shown that A-RoF based system is capable of supporting 5G signals with an acceptable degradation of QoS. For example in [16], we experimentally verified that the A-RoF system is capable of supporting a $2 \times 2$ MIMO system with less than 1 dB SNR degradation compared to the traditional system.

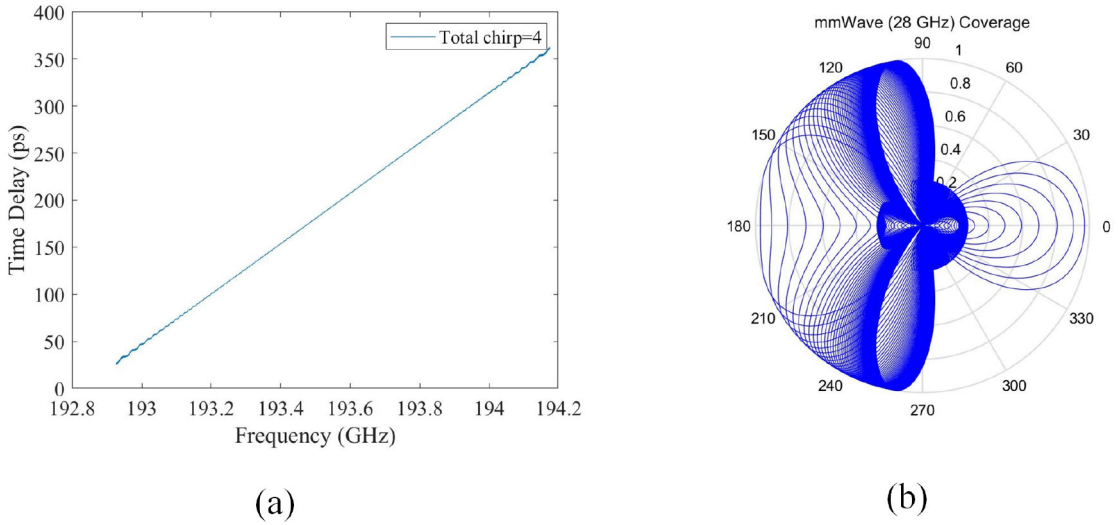


**FIGURE 5.** The Time Delay and its Corresponding Beam coverage.

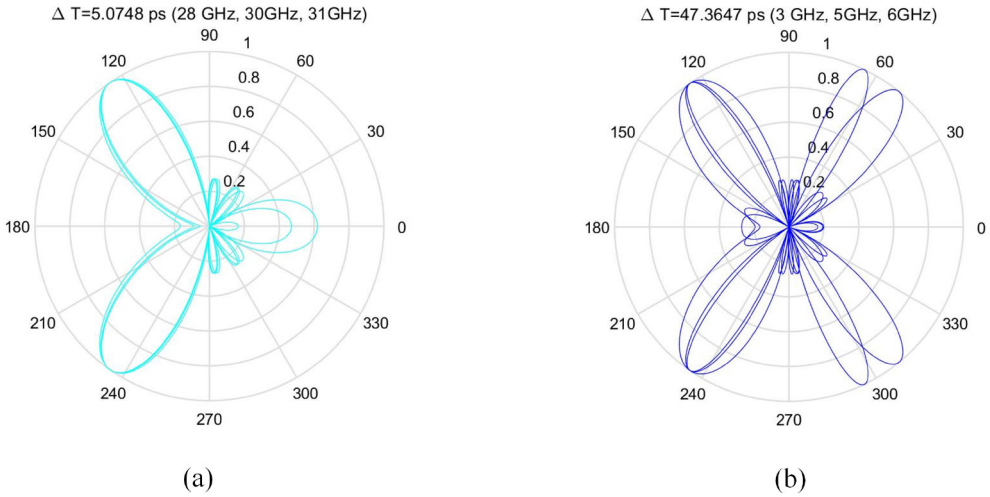


**FIGURE 6.** Multi-service Beam in the same direction. (a) The beam direction of mmWave signals at 28 GHz, 30 GHz and 31 GHz, when the true-time-delay $\Delta T$ of Section III-B is 5.0748. (b) The beam direction of sub-6GHz signals at 3 GHz, 5 GHz and 6 GHz, when the true-time-delay $\Delta T$ of Section III-B is 47.3647.

optical community. We directly modulate the laser diode using different frequencies of $f_1 = 3, f_2 = 5$ and $f_3 = 6$ GHz, where an arbitrary wavelength generator (AWG) can be used. Then, after the true-time-delay process using the chirped-FBGs detailed in Section III-B, and the optical interleaver, a photonic RF generation of sub-6GHz at $f_1 = 3$, $f_2 = 5$ and $f_3 = 6$ GHz and mmWave at $f_1 + \frac{\Delta f}{2} = 28$, $f_2 + \frac{\Delta f}{2} = 30$ and $f_3 + \frac{\Delta f}{2} = 31$ GHz can be obtained without the need for the bulky and high-energy consuming RF mixers, where $\Delta f = \Delta f_1 = \Delta f_2$. In this system, a DWDM mux and demux are used for combining the different services over the fiber as well as for separating the individual services to the on-board passengers.

In this section, we present our novel beamforming design, where we obtain a relation between the optical signal after the CFBG1 and CFBG2 in the CU of Fig. 4 and its time delay imposed in Fig. 5(a). Explicitly, as portrayed in Fig. 5 by tuning a supported beam's deflection as detailed in [31], we are capable of changing the total chirp, which results in a linear relation between the time-delay and the optical frequency as depicted in Fig. 5(a). Hence this results in a multi-service beam coverage around 180° as shown in Fig. 5(b).

Moreover, to prove that our design can provide the same directional beam for both sub-6GHz and mmWave spectrum, as analysed in Section III, the CFBG1 and CFBG2 of Fig. 3 are required to impose the same degree of time-delay difference, while CFBG 3 is tuned to a time-delay value related to the CFBG 1 and CFBG 2. As shown in Fig 6, the sub-6GHz beams are directed to the same direction as the mmWave beam, when $\Delta T_1 = 47.3647$ and $\Delta T_2 = 5.0748$, where the relationship is $\Delta T_1 = d_2 * \Delta T_2 / d_1$. In our example, $d_1 = \lambda_{3GHz}/2$ and $d_2 = \lambda_{28GHz}/2$ are the inter-element distances of the sub-6GHz antenna array and mmWave antenna

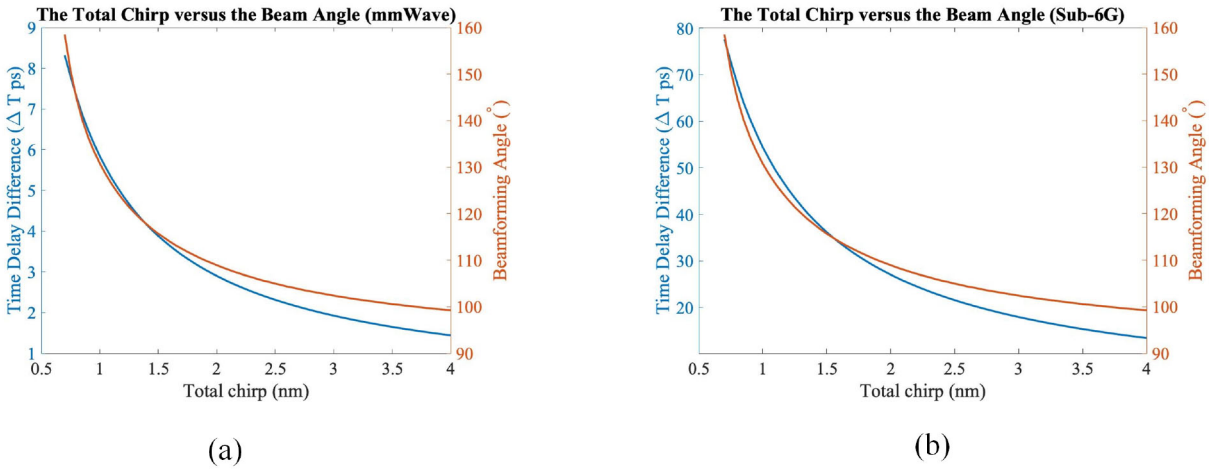


**FIGURE 7.** The total chirp versus the beam angle.

array, respectively, where we assume the center frequencies are 3 GHz and 28 GHz. Hence we have $d_2/d_1 = 0.107$.

Furthermore, it is shown in Fig. 7(a) and (b) that the sub-6GHz and mmWave signal can be mapped to the same beamforming angle, thanks to the introduction of CFBG 3 in the RRH of Fig. 3. When the total chirp of both the CFBG 1 and CFBG 2 ranges from 0.7 to 4 nm with a step-size of 0.05, the time delay difference of the sub-6GHz and mmWave signals spans from 77.6 ps to 13.4 ps and from 8.3 to 1.4 ps, respectively, which results in a beam angle from 158.48° to 99.23 ° as shown in Fig. 7(a) and (b). Thus, by controlling the total chirp of the CFBG 3 in the RRH according to the total chirp in the CU, we can direct the multi-service signal to the same direction as shown in Fig. 6.

Then, as shown in Fig. 6(b) and Fig. 5, the corresponding multi-service beam coverage, which is around 180° with a high precision, verifies that our photonic beamforming system can radiate the wideband beam flexibly and widely, while substantially simplifying the RRH designs as analysed in Section III.

## V. CONCLUSION

In this article, we have proposed a low-cost A-RoF aided multi-service communications in the two-hop relay train system, where we implemented the photonic beamformer using the CFBGs, enabling a centralised and low-cost RAN design. In this paper, we designed a double time-delay mapping rule of the optical signals and the corresponding RF signals and verified that the proposed system was capable of reducing the total cost of the RAN by simplifying the RRHs. Finally, a single beam transmitting the multi-service signals with a 180° beamforming range was presented.

## REFERENCES

[1] J. Kim *et al.*, "A comprehensive study on mmWave-based mobile hotspot network system for high-speed train communications," *IEEE Trans. Veh. Technol.*, vol. 68, no. 3, pp. 2087–2101, Mar. 2019.

[2] B. L. Dang, M. G. Larrode, R. V. Prasad, I. Niemegeers, and A. Koonen, "Radio-over-fiber based architecture for seamless wireless indoor communication in the 60 GHz band," *Comput. Commun.*, vol. 30, no. 18, pp. 3598–3613, 2007.

[3] A. Osseiran, J. F. Monserrat, and P. Marsch, *5G Mobile and Wireless Communications Technology*. Cambridge, U.K.: Cambridge Univ. Press, 2016.

[4] A. Kanno *et al.*, "High-speed railway communication system using linear-cell-based radio-over-fiber network and its field trial in 90-GHz bands," *J. Lightw. Technol.*, vol. 38, no. 1, pp. 112–122, Jan. 1, 2020.

[5] J. D. Oliva Sánchez and J. I. Alonso, "A two-hop MIMO relay architecture using LTE and millimeter wave bands in high-speed trains," *IEEE Trans. Veh. Technol.*, vol. 68, no. 3, pp. 2052–2065, Mar. 2019.

[6] Y. Li, M. El-Hajjar, and L. Hanzo, "Joint space-time block-coding and beamforming for the multi-user radio over plastic fiber downlink," *IEEE Trans. Veh. Technol.*, vol. 67, no. 3, pp. 2781–2786, Mar. 2018.

[7] A. Goldsmith, *Wireless Communications*. Cambridge, U.K.: Cambridge Univ. Press, 2005.

[8] L. Hanzo, H. Haas, S. Imre, D. O'Brien, M. Rupp, and L. Gyongyosi, "Wireless myths, realities, and futures: From 3G/4G to optical and quantum wireles," *Proc. IEEE*, vol. 100, pp. 1853–1888, May 2012, doi: 10.1109/JPROC.2012.2189788.

[9] P. T. Dat, A. Kanno, N. Yamamoto, and T. Kawanishi, "WDM RoF-MMW and linearly located distributed antenna system for future high-speed railway communications," *IEEE Commun. Mag.*, vol. 53, no. 10, pp. 86–94, Oct. 2015.

[10] I. A. Hemadeh, K. Satyanarayana, M. El-Hajjar, and L. Hanzo, "Millimeter-wave communications: Physical channel models, design considerations, antenna constructions, and link-budget," *IEEE Commun. Surveys Tuts.*, vol. 20, no. 2, pp. 870–913, 2nd Quart., 2018.

[11] A. Checko *et al.*, "Cloud RAN for mobile networks—A technology overview," *IEEE Commun. Surveys Tuts.*, vol. 17, no. 1, pp. 405–426, 1st Quart., 2015.

[12] A. Alkhateeb, J. Mo, N. Gonzalez-Prelcic, and R. W. Heath, "MIMO precoding and combining solutions for millimeter-wave systems," *IEEE Commun. Mag.*, vol. 52, no. 12, pp. 122–131, Dec. 2014.

[13] V. A. Thomas, M. El-Hajjar, and L. Hanzo, "Millimeter-wave radio over fiber optical upconversion techniques relying on link nonlinearity," *IEEE Commun. Surveys Tuts.*, vol. 18, no. 1, pp. 29–53, 1st Quart., 2016.

[14] Y. Li, F. Wang, M. El-Hajjar, and L. Hanzo, "Analog radio-over-fiber-aided optical-domain MIMO signal processing for high-performance low-cost radio access networks," *IEEE Commun. Mag.*, vol. 59, no. 1, pp. 126–132, Jan. 2021.

[15] Z. Cao *et al.*, "Advanced integration techniques on broadband millimeter-wave beam steering for 5G wireless networks and beyond," *IEEE J. Quantum Electron.*, vol. 52, no. 1, pp. 1–20, Jan. 2016.

[16] Y. Li, Q. Yang, I. A. Hemadeh, M. El-Hajjar, C.-K. Chan, and L. Hanzo, "Experimental characterization of the radio over fiber aided twin-antenna spatial modulation downlink," *Opt. Exp.*, vol. 26, no. 10, pp. 12432–12440, May 2018.

[17] Y. Li, I. A. Hemadeh, M. El-Hajjar, and L. Hanzo, "Radio over fiber downlink design for spatial modulation and multi-set space-time shift-keying," *IEEE Access*, vol. 6, pp. 21812–21827, 2018.
[18] V. Thomas, M. El-Hajjar, and L. Hanzo, "Performance improvement and cost reduction techniques for radio over fiber communications," *IEEE Commun. Surveys Tuts.*, vol. 17, no. 2, pp. 627–670, 2nd Quart., 2015.
[19] Y. Li, S. Ghafoor, K. Satyanarayana, M. El-Hajjar, and L. Hanzo, "Analogue wireless beamforming exploiting the fiber-nonlinearity of radio over fiber-based C-RANs," *IEEE Trans. Veh. Technol.*, vol. 68, no. 3, pp. 2802–2813, Mar. 2019.
[20] G. Vasileiou, G. I. Papadimitriou, P. Nicopolitidis, and P. G. Sarigiannidis, "An effective resource allocation medium access control protocol for radio-over-fiber access networks based on wavelength reuse," *Comput. Commun.*, vol. 88, pp. 45–56, Aug. 2016.
[21] A. Molony, L. Zhang, J. Willlams, I. Bennion, C. Edge, and J. Fells, "Fiber Bragg grating networks for time-delay control of phased-array antennas," presented at the Conf. Lasers Electro-Opt., 1996, pp. 244–245.
[22] G. A. Ball, W. H. Glenn, and W. W. Morey, "Programmable fiber optic delay line," *IEEE Photon. Technol. Lett.*, vol. 6, no. 6, pp. 741–743, Jun. 1994.
[23] D. B. Hunter, M. E. Parker, and J. L. Dexter, "Demonstration of a continuously variable true-time delay beamformer using a multichannel chirped fiber grating," *IEEE Trans. Microw. Theory Techn.*, vol. 54, no. 2, pp. 861–867, Feb. 2006.
[24] J. Yao, J. Yang, and Y. Liu, "Continuous true-time-delay beamforming employing a multiwavelength tunable fiber laser source," *IEEE Photon. Technol. Lett.*, vol. 14, no. 5, pp. 687–689, May 2002.
[25] J. S. Wey, Y. Luo, and T. Pfeiffer, "5G wireless transport in a PON context: An overview," *IEEE Commun. Stand. Mag.*, vol. 4, no. 1, pp. 50–56, Mar. 2020.
[26] *Common Public Radio Interface: eCPRI Interface Specification eCPRI Specification V2.0*, eCPRI, Bangalore, India, May 2019.
[27] A. Udalcovs *et al.*, "Total cost of ownership of digital vs. analog radio-over-fiber architectures for 5G fronthauling," *IEEE Access*, vol. 8, pp. 223562–223573, 2020.
[28] J. Wang, H. Zhu, and N. J. Gomes, "Distributed antenna systems for mobile communications in high speed trains," *IEEE J. Sel. Areas Commun.*, vol. 30, no. 4, pp. 675–683, May 2012.
[29] G. Liu, Y. Huang, Z. Chen, L. Liu, Q. Wang, and N. Li, "5G deployment: Standalone vs. non-standalone from the operator perspective," *IEEE Commun. Mag.*, vol. 58, no. 11, pp. 83–89, Nov. 2020.
[30] T. Han and N. Ansari, "Radiate: Radio over fiber as an antenna extender for high-speed train communications," *IEEE Wireless Commun.*, vol. 22, no. 1, pp. 130–137, Feb. 2015.
[31] Y. Liu, J. Yang, and J. Yao, "Continuous true-time-delay beamforming for phased array antenna using a tunable chirped fiber grating delay line," *IEEE Photon. Technol. Lett.*, vol. 14, no. 8, pp. 1172–1174, Aug. 2002.
[32] F. Ellinger *et al.*, "Integrated adjustable phase shifters," *IEEE Microw. Mag.*, vol. 11, no. 6, pp. 97–108, Oct. 2010.
[33] M. Cai *et al.*, "Effect of wideband beam squint on codebook design in phased-array wireless systems," in *Proc. IEEE Global Commun. Conf. (GLOBECOM)*, 2016, pp. 1–6.
[34] B. Wang, M. Jian, F. Gao, G. Y. Li, and H. Lin, "Beam squint and channel estimation for wideband mmwave massive MIMO-OFDM systems," *IEEE Trans. Signal Process.*, vol. 67, no. 23, pp. 5893–5908, Dec. 2019.
[35] Y. Li, K. Satyanarayana, M. El-Hajjar, and L. Hanzo, "Analogue radio over fiber aided mimo design for the learning assisted adaptive C-RAN downlink," *IEEE Access*, vol. 7, pp. 21359–21371, 2019.
[36] D. Perez-Galacho, D. Sartiano, and S. Sales, "Fronthaul links based on analog radio over fiber," in *Proc. Eur. Conf. Netw. Commun. (EuCNC)*, 2019, pp. 475–478.
[37] M. Sung *et al.*, "Demonstration of 5G trial service in 28 GHz millimeter wave using IFoF-based analog distributed antenna system," in *Proc. Opt. Fiber Commun. Conf. Exhibition (OFC)*, 2019, pp. 1–3.

**YICHUAN LI** received the B.Sc. degree in optics information science and technology from the China University of Petroleum (East China), Qingdao, China, in 2012, and the M.Sc. and Ph.D. degrees in wireless communications from the University of Southampton, Southampton, UK., in 2014 and 2019, respectively. He is an Assistant Professor with the Harbin Institute of Technology (Shenzhen), Shenzhen, China. He was a Research Assistant with the Lightwave Communication Laboratory, Chinese University of Hong Kong from July to October 2017. His research is focused on the radio over fiber for backhaul, fronthaul, and indoor communication network. His research interests are millimeter-wave over fiber, optical fiber-aided analog beamforming techniques, multifunctional MIMO, mode-division multiplexing in multimode fiber, and fiber-based C-RAN system.

**SALMAN GHAFOOR** received the B.Sc. degree in electrical engineering from UET Peshawar, Peshawar, Pakistan, in 2006, the M.Sc. degree in electronic communications and computer engineering from the University of Nottingham, Nottingham, U.K., and the Ph.D. degree from the School of Electronics and Computer Science, University of Southampton, Southampton, U.K., in 2012, where he was a Research Student with Optoelectronics Research Centre for two years. He is currently an Associate Professor with the National University of Sciences and Technology, Islamabad, Pakistan. His areas of research include free-space optical communications, all-optical signal processing, ultrawideband over fiber, and radio over fiber systems.

**MOHAMMED EL-HAJJAR** (Senior Member, IEEE) received the Ph.D. degree in wireless communications from the University of Southampton, U.K., in 2008, where he is an Associate Professor with the School of Electronics and Computer Science. Following the Ph.D. degree, he joined Imagination Technologies as a Design Engineer, where he worked on designing and developing Imagination's multistandard communications platform, which resulted in three patents. He is the recipient of several academic awards and has published a Wiley–IEEE book and in excess of 80 journal and conference papers. His research interests include the development of intelligent communications systems, energy-efficient transceiver design, MIMO, millimeter-wave communications, and radio over fiber network design.